# DGFEM for dynamical systems describing interaction of compressible fluid and structures

Miloslav Feistauer[a,b], Jaroslava Hasnedlová-Prokopová[a], Jaromír Horáček[b], Adam Kosík[a], Václav Kučera[a]

[a] *Charles University Prague, Faculty of Mathematics and Physics, Sokolovská 83, 186 75 Praha 8, Czech Republic*
[b] *Institute of Thermomechanics, Academy of Sciences of the Czech Republic, Dolejškova 5, 182 00 Praha 8, Czech Republic*

**Abstract**

The paper is concerned with the numerical solution of flow-induced vibrations of elastic structures. The dependence on time of the domain occupied by the fluid is taken into account with the aid of the ALE (Arbitrary Lagrangian-Eulerian) formulation of the compressible Navier-Stokes equations. The deformation of the elastic body, caused by aeroelastic forces, is described by the linear dynamical elasticity equations. These two systems are coupled by transmission conditions. The flow problem is discretized by the discontinuous Galerkin finite element method (DGFEM) in space and by the backward difference formula (BDF) in time. The structural problem is discretized by conforming finite elements and the Newmark method. The fluid-structure interaction is realized via weak or strong coupling algorithms. The developed technique is tested by numerical experiments and applied to the simulation of vibrations of vocal folds during phonation onset.

*Keywords:* compressible Navier-Stokes equations, time dependent domain, ALE method, discontinuous Galerkin method, semi-implicit time discretization, dynamic elasticity equations, conforming finite elements, Newmark method, weak and strong coupling, flow in glottis, flow-induced vibrations of vocal folds.

*Email addresses:* feist@karlin.mff.cuni.cz (Miloslav Feistauer), jarkaprokop@post.cz (Jaroslava Hasnedlová-Prokopová), jaromirh@it.cas.cz (Jaromír Horáček), adam.kosik@atlas.cz (Adam Kosík), vaclav.kucera@email.cz (Václav Kučera)

*2000 MSC:* 65M60, 76M10, 76N15

## 1. Introduction

The studies on flow-induced vibrations play an important role in a number of fields in science and technology (e.g., vibrations of airplane wings or turbine blades, interaction of wind with bridges, TV towers or cooling towers of power stations) but also in biomechanics, e.g., simulation of the vocal folds vibrations and voice production. In all of these examples the moving medium is gas, i.e. compressible fluid. For low Mach number flows incompressible models are used (as e.g. in [3], [12]), but in some cases compressibility plays an important role.

The goal of our research is the numerical finite element (FE) simulation of interaction of compressible 2D viscous flow in the glottal region with a compliant tissue of the human vocal folds modeled by a 2D elastic layered structure. A current challenging question is a mathematical and physical description of the mechanism for transforming the airflow energy in the glottis into the acoustic energy representing the voice source in humans. The primary voice source is given by the airflow coming from the lungs that causes self-oscillations of the vocal folds. The voice source signal travels from the glottis to the mouth, exciting the acoustic supraglottal spaces, and becomes modified by acoustic resonance properties of the vocal tract ([13]).

An overview [2] presents the current state of mathematical models for the human phonation process. In current publications various simplified glottal flow models are used. They are based on the Bernoulli equation ([13]), 1D models for an incompressible inviscid fluid ([9]), 2D incompressible Navier-Stokes equations solved by the finite volume method ([1]) or finite element method ([15]). Acoustic wave propagation in the vocal tract is usually modelled separately using linear acoustic perturbation theory ([14]). Work [11] is concerned with the finite volume solution of the Navier-Stokes equations for a compressible fluid with prescribed periodic changes of the channel cross-section of the glottal channel. The phonation onset was studied by using the potential flow model and three-mass lumped model for the vibrating vocal folds in [8] and for a 2D isotropic elastic model of the vocal folds in [16].

The present paper is devoted to the numerical simulation of vocal folds vibrations induced by compressible viscous flow. The air flow is described by the compressible Navier-Stokes equations written in the arbitrary Lagrangian-Eulerian (ALE) form in order to take into account the time dependence of

the domain occupied by the air. The vocal folds are considered as isotropic elastic bodies. Their vibrations are described by the linear elasticity equations. The coupled fluid-structure interaction problem represents a strongly nonlinear dynamical system, which is analyzed numerically.

The flow problem is discretized in space by the discontinuous Galerkin finite element method (DGFEM), using piecewise polynomial approximations, in general discontinuous on interfaces between neighbouring elements. The time discretization is carried out by the backward difference formula (BDF) in time. The structural problem is approximated by conforming finite elements and the Newmark method. The fluid-structure interaction is realized via weak or strong coupling algorithms.

The contents of the paper is the following. In Section 2, the continuous fluid-structure interaction (FSI) problem is formulated. Section 3 is concerned with the derivation of the discrete problem. Section 4 is devoted to the realization of the coupled FSI problem. It consists of the construction of the ALE mapping and the formulation of the coupling algorithms. In Section 5, we present results of numerical tests showing the applications to the simulation of flow-induced vibrations of vocal folds. In Conclusion, subjects for future work are formulated.

## 2. Continuous problem

In this section we shall formulate the problem of the interaction of a compressible flow with an elastic structure.

### *2.1. Formulation of the flow problem*

We consider a compressible flow in a bounded domain $\Omega_t \subset I\!R^2$ depending on time $t \in [0, T]$. We assume that the boundary of $\Omega_t$ is formed by three disjoint parts: $\partial\Omega_t = \Gamma_I \cup \Gamma_O \cup \Gamma_{W_t}$, where $\Gamma_I$ is the inlet, $\Gamma_O$ is the outlet and $\Gamma_{W_t}$ denotes impermeable walls that may move in dependence on time.

The dependence of the domain $\Omega_t$ on time is taken into account with the use of the *arbitrary Lagrangian-Eulerian* (ALE) method, see e.g. [10]. It is based on a regular one-to-one ALE mapping of the reference configuration $\Omega_0$ onto the current configuration $\Omega_t$:

$$\mathcal{A}_t : \overline{\Omega}_0 \longrightarrow \overline{\Omega}_t, \ i.e. \ \boldsymbol{X} \in \overline{\Omega}_0 \longmapsto \boldsymbol{x} = \boldsymbol{x}(\boldsymbol{X}, t) = \mathcal{A}_t(\boldsymbol{X}) \in \overline{\Omega}_t.$$

We define the domain velocity:

$$\begin{aligned} \tilde{\boldsymbol{z}}(\boldsymbol{X},t) &= \frac{\partial}{\partial t}\mathcal{A}_t(\boldsymbol{X}), \quad t\in[0,T],\ \boldsymbol{X}\in\Omega_0, \\ \boldsymbol{z}(\boldsymbol{x},t) &= \tilde{\boldsymbol{z}}(\mathcal{A}^{-1}(\boldsymbol{x}),t), \quad t\in[0,T],\ \boldsymbol{x}\in\Omega_t \end{aligned} \tag{1}$$

and the ALE derivative of the vector function $\boldsymbol{w}=\boldsymbol{w}(\boldsymbol{x},t)$ defined for $\boldsymbol{x}\in\Omega_t$ and $t\in[0,T]$:

$$\frac{D^A}{Dt}\boldsymbol{w}(\boldsymbol{x},t)=\frac{\partial\tilde{\boldsymbol{w}}}{\partial t}(\boldsymbol{X},t), \tag{2}$$

where

$$\tilde{\boldsymbol{w}}(\boldsymbol{X},t)=\boldsymbol{w}(\mathcal{A}_t(\boldsymbol{X}),t),\ \boldsymbol{X}\in\Omega_0,\ \boldsymbol{x}=\mathcal{A}_t(\boldsymbol{X}).$$

Then, using the relations

$$\frac{D^A w_i}{Dt}=\frac{\partial w_i}{\partial t}+\operatorname{div}(\boldsymbol{z}w_i)-w_i\operatorname{div}\boldsymbol{z}, \quad i=1,\dots,4,$$

we can write the governing system consisting of the continuity equation, the Navier-Stokes equations and the energy equation in the ALE form

$$\frac{D^A\boldsymbol{w}}{Dt}+\sum_{s=1}^{2}\frac{\partial\boldsymbol{g}_s(\boldsymbol{w})}{\partial x_s}+\boldsymbol{w}\operatorname{div}\boldsymbol{z}=\sum_{s=1}^{2}\frac{\partial\boldsymbol{R}_s(\boldsymbol{w},\nabla\boldsymbol{w})}{\partial x_s}. \tag{3}$$

See, for example [6]. Here

$$\begin{aligned} \boldsymbol{w} &= (w_1,\dots,w_4)^T=(\rho,\rho v_1,\rho v_2,E)^T\in\mathbb{R}^4, \\ \boldsymbol{w} &= \boldsymbol{w}(x,t),\ x\in\Omega_t,\ t\in(0,T), \\ \boldsymbol{g}_s(\boldsymbol{w}) &= \boldsymbol{f}_s(\boldsymbol{w})-z_s\boldsymbol{w}, \quad s=1,2, \\ \boldsymbol{f}_i(\boldsymbol{w}) &= (f_{i1},\cdots,f_{i4})^T=(\rho v_i,\rho v_1v_i+\delta_{1i}\,p,\rho v_2v_i+\delta_{2i}\,p,(E+p)v_i)^T, \\ \boldsymbol{R}_i(\boldsymbol{w},\nabla\boldsymbol{w}) &= (R_{i1},\dots,R_{i4})^T=\left(0,\tau_{i1}^V,\tau_{i2}^V,\tau_{i1}^V\,v_1+\tau_{i2}^V\,v_2+k\partial\theta/\partial x_i\right)^T, \\ \tau_{ij}^V &= \lambda\operatorname{div}\boldsymbol{v}\,\delta_{ij}+2\mu\,d_{ij}(\boldsymbol{v}),\ d_{ij}(\boldsymbol{v})=\frac{1}{2}\left(\frac{\partial v_i}{\partial x_j}+\frac{\partial v_j}{\partial x_i}\right). \end{aligned} \tag{4}$$

We use the following notation: $\rho$ – density, $p$ – pressure, $E$ – total energy, $\boldsymbol{v}=(v_1,v_2)$ – velocity, $\theta$ – absolute temperature, $\gamma>1$ – Poisson adiabatic constant, $c_v>0$ – specific heat at constant volume, $\mu>0,\lambda=-2\mu/3$ – viscosity coefficients, $k$ – heat conduction, $\tau_{ij}^V$ – components of the viscous part of the stress tensor. The vector-valued function $\boldsymbol{w}$ is called state vector,

the functions $\boldsymbol{f}_i$ are the so-called inviscid fluxes and $\boldsymbol{R}_i$ represent viscous terms. The above system is completed by the thermodynamical relations

$$p = (\gamma - 1)(E - \frac{1}{2}\rho|\boldsymbol{v}|^2), \quad \theta = \frac{1}{c_v}\Big(\frac{E}{\rho} - \frac{1}{2}|\boldsymbol{v}|^2\Big). \tag{5}$$

The resulting system is equipped with the initial condition

$$\boldsymbol{w}(x,0) = \boldsymbol{w}^0(x), \quad x \in \Omega_0, \tag{6}$$

and the following boundary conditions:

$$\begin{aligned}
&\text{a)}\ \ \rho|_{\Gamma_I} = \rho_D, \quad \text{b)}\ \ \boldsymbol{v}|_{\Gamma_I} = \boldsymbol{v}_D = (v_{D1}, v_{D2})^{\mathrm{T}}, \\
&\text{c)}\ \ \sum_{i,j=1}^{2} \tau_{ij}^V n_i v_j + k\frac{\partial\theta}{\partial n} = 0 \quad \text{on } \Gamma_I, \\
&\text{d)}\ \ \boldsymbol{v}|_{\Gamma_{W_t}} = \boldsymbol{z}_D = \text{velocity of a moving wall}, \ \text{e)}\ \ \frac{\partial\theta}{\partial n}|_{\Gamma_{W_t}} = 0 \text{ on } \Gamma_{W_t}, \\
&\text{f)}\ \ \sum_{i=1}^{2} \tau_{ij}^V n_i = 0, \quad j = 1,\, 2, \quad \text{g)}\ \ \frac{\partial\theta}{\partial n} = 0 \text{ on } \Gamma_O,
\end{aligned} \tag{7}$$

with prescribed data $\rho_D, \boldsymbol{v}_D$ and $\boldsymbol{z}_D$.

*2.2. Elasticity problem and fluid-structure interaction coupling*

For the description of the deformation of an elastic structure we shall use the model of dynamical linear elasticity formulated in a bounded open set $\Omega^b \subset \mathbb{R}^2$ representing the elastic body, which has a common boundary with the reference domain $\Omega_0$ occupied by the fluid at the initial time. We denote by $\boldsymbol{u}(\boldsymbol{X},t) = (u_1(\boldsymbol{X},t), u_2(\boldsymbol{X},t)$, $\boldsymbol{X} = (X_1, X_2) \in \Omega^b$, $t \in (0,T)$, the displacement of the body. The equations describing the deformation of the elastic body $\Omega^b$ have the form

$$\varrho^b\frac{\partial^2 u_i}{\partial t^2} + C\varrho^b\frac{\partial u_i}{\partial t} - \sum_{j=1}^{2}\frac{\partial\tau_{ij}^b}{\partial X_j} = 0 \quad \text{in } \Omega^b \times (0,T), \quad i = 1,2. \tag{8}$$

Here $\tau_{ij}^b$ are the components of the stress tensor defined by the generalized Hooke's law for isotropic bodies

$$\tau_{ij}^b = \lambda^b \mathrm{div}\,\boldsymbol{u}\,\delta_{ij} + 2\mu^b e_{ij}^b(\boldsymbol{u}), \quad i,j = 1,2. \tag{9}$$

By $\boldsymbol{e}^b = \{e_{ij}^b\}_{i,j=1}^2$ we denote the strain tensor defined by

$$e_{ij}^b(\boldsymbol{u}) = \frac{1}{2}\left(\frac{\partial u_i}{\partial X_j} + \frac{\partial u_j}{\partial X_i}\right), \quad i,j = 1,2. \tag{10}$$

The Lamé coefficients $\lambda^b$ and $\mu^b$ are related to the Young modulus $E^b$ and the Poisson ratio $\sigma^b$ as

$$\lambda^b = \frac{E^b\sigma^b}{(1+\sigma^b)(1-2\sigma^b)}, \quad \mu^b = \frac{E^b}{2(1+\sigma^b)}, \tag{11}$$

The expression $C\varrho^b\frac{\partial u_i}{\partial t}$, where $C \geq 0$, is the dissipative structural damping of the system and $\varrho^b$ denotes the material density.

We complete the elasticity problem by initial and boundary conditions. The initial conditions read

$$\boldsymbol{u}(\cdot,0) = \boldsymbol{0}, \quad \frac{\partial \boldsymbol{u}}{\partial t}(\cdot,0) = \boldsymbol{0}, \quad \text{in } \Omega^b. \tag{12}$$

Further, we assume that $\partial\Omega^b = \Gamma_W^b \cup \Gamma_D^b$, where $\Gamma_W^b$ and $\Gamma_D^b$ are two disjoints parts of $\partial\Omega^b$. We assume that $\Gamma_W^b$ is a common part between the fluid and structure at time $t = 0$. This means that $\Gamma_W^b \subset \Gamma_{W_0}$. On $\Gamma_W^b$ we prescribe the normal component of the stress tensor and assume that the part $\Gamma_D^b$ is fixed. This means that the following boundary conditions are used:

$$\sum_{j=1}^{2} \tau_{ij}^b n_j = T_i^{\boldsymbol{n}} \quad \text{on } \Gamma_W^b \times (0,T), \quad i = 1,2, \tag{13}$$

$$\boldsymbol{u} = 0 \quad \text{on } \Gamma_D^b \times (0,T). \tag{14}$$

By $\boldsymbol{T^n} = (T_1^n, T_2^n)$ we denote the prescribed normal component of the stress tensor.

The structural problem consists in finding the displacement $\boldsymbol{u}$ satisfying equations (8) and the initial and boundary conditions (12) – (14).

Now we shall deal with the formulation of the coupled FSI problem. We denote the common boundary between the fluid and the structure at time $t$ by $\tilde{\Gamma}_{W_t}$. It is given by

$$\tilde{\Gamma}_{W_t} = \left\{\boldsymbol{x} \in \mathbb{R}^2;\ \boldsymbol{x} = \boldsymbol{X} + \boldsymbol{u}(\boldsymbol{X},t),\ \boldsymbol{X} \in \Gamma_W^b\right\}. \tag{15}$$

Thus, the domain $\Omega_t$ is determined by the displacement $\boldsymbol{u}$ of the part $\Gamma_W^b$ at time $t$. The ALE mapping $\mathcal{A}_t$ is constructed with the aid of a special stationary linear elasticity problem - see Section 4.1.

If the domain $\Omega_t$ occupied by the fluid at time $t$ is known, we can solve the problem describing the flow and compute the surface force acting onto the body on the interface $\tilde{\Gamma}_{W_t}$, which can be transformed to the reference configuration, i.e. to the interface $\Gamma^b_W$. In case of the linear elasticity model, when only small deformations are considered, we get the transmission condition

$$\sum_{j=1}^{2} \tau^b_{ij}(\boldsymbol{X}) n_j(\boldsymbol{X}) = -\sum_{j=1}^{2} \tau^f_{ij}(\boldsymbol{x}) n_j(\boldsymbol{X}), \quad i = 1, 2, \tag{16}$$

where $\tau^f_{ij}$ are the components of the stress tensor of the fluid:

$$\tau^f_{ij} = -p\delta_{ij} + \tau^V_{ij}, \quad i, j = 1, 2, \tag{17}$$

the points $\boldsymbol{x}$ and $\boldsymbol{X}$ satisfy the relation

$$\boldsymbol{x} = \boldsymbol{X} + \boldsymbol{u}(\boldsymbol{X}, t). \tag{18}$$

and $\boldsymbol{n}(\boldsymbol{X}) = (n_1(\boldsymbol{X}), n_2(\boldsymbol{X}))$ denotes the unit outer normal to the body $\Omega^b$ on $\Gamma^b_W$ at the point $\boldsymbol{X}$. Further, the fluid velocity is defined on the moving part of the boundary $\tilde{\Gamma}_{W_t}$ by the second transmission condition

$$\boldsymbol{v}(\boldsymbol{x}, t) = \boldsymbol{z}_D(\boldsymbol{x}, t) = \frac{\partial \boldsymbol{u}(\boldsymbol{X}, t)}{\partial t}. \tag{19}$$

Now we formulate the *continuous FSI problem*: We want to determine the domain $\Omega_t$, $t \in (0, T]$ and functions $\boldsymbol{w} = \boldsymbol{w}(\boldsymbol{x}, t)$, $\boldsymbol{x} \in \overline{\Omega}_t$, $t \in [0, T]$ and $\boldsymbol{u} = \boldsymbol{u}(\boldsymbol{X}, t)$, $\boldsymbol{X} \in \overline{\Omega}^b$, $t \in [0, T]$ satisfying equations (3), (8), the initial conditions (6), (12), the boundary conditions (7), (13), (14) and the transmission conditions (16), (19).

This FSI problem represents a strongly nonlinear dynamical system. Theoretical analysis of qualitative properties of this problem, as the existence, uniqueness and regularity of its solution, is open. Therefore, in the sequel we shall be concerned with its numerical solution.

## 3. Discrete problem

First we describe numerical methods for the solution of separately considered flow and structural problems.

*3.1. Discretization of the flow problem*

*3.1.1. Space discretization*

For the space semidiscretization we use the discontinuous Galerkin finite element method (DGFEM). We construct a polygonal approximation $\Omega_{ht}$ of the domain $\Omega_t$. By $\mathcal{T}_{ht}$ we denote a partition of the closure $\overline{\Omega}_{ht}$ of the domain $\Omega_{ht}$ into a finite number of closed triangles $K$ with mutually disjoint interiors such that $\overline{\Omega}_{ht} = \bigcup_{K\in\mathcal{T}_{ht}} K$.

By $\mathcal{F}_{ht}$ we denote the system of all faces of all elements $K \in \mathcal{T}_{ht}$. Further, we introduce the set of all interior faces $\mathcal{F}_{ht}^I = \{\Gamma \in \mathcal{F}_{ht};\ \Gamma \subset \Omega_t\}$, the set of all boundary faces $\mathcal{F}_{ht}^B = \{\Gamma \in \mathcal{F}_{ht};\ \Gamma \subset \partial\Omega_{ht}\}$ and the set of all "Dirichlet" boundary faces $\mathcal{F}_{ht}^D = \left\{\Gamma \in \mathcal{F}_{ht}^B;\ \text{a Dirichlet condition is prescribed on } \Gamma\right\}$. Each $\Gamma \in \mathcal{F}_{ht}$ is associated with a unit normal vector $\boldsymbol{n}_\Gamma$ to $\Gamma$. For $\Gamma \in \mathcal{F}_{ht}^B$ the normal $\boldsymbol{n}_\Gamma$ has the same orientation as the outer normal to $\partial\Omega_{ht}$. We set $d(\Gamma) =$ length of $\Gamma \in \mathcal{F}_{ht}$.

For each $\Gamma \in \mathcal{F}_{ht}^I$ there exist two neighbouring elements $K_\Gamma^{(L)}, K_\Gamma^{(R)} \in \mathcal{T}_{ht}$ such that $\Gamma \subset \partial K_\Gamma^{(R)} \cap \partial K_\Gamma^{(L)}$. We use the convention that $K_\Gamma^{(R)}$ lies in the direction of $\boldsymbol{n}_\Gamma$ and $K_\Gamma^{(L)}$ lies in the opposite direction to $\boldsymbol{n}_\Gamma$. If $\Gamma \in \mathcal{F}_{ht}^B$, then the element adjacent to $\Gamma$ will be denoted by $K_\Gamma^{(L)}$.

The approximate solution will be sought in the space of piecewise polynomial functions

$$\boldsymbol{S}_{ht} = [S_{ht}]^4, \quad \text{with} \quad S_{ht} = \{v; v|_K \in P_r(K)\ \forall\, K \in \mathcal{T}_{ht}\}, \tag{20}$$

where $r \geq 1$ is an integer and $P_r(K)$ denotes the space of all polynomials on $K$ of degree $\leq r$. A function $\boldsymbol{\varphi} \in \boldsymbol{S}_{ht}$ is, in general, discontinuous on interfaces $\Gamma \in \mathcal{F}_{ht}^I$. By $\boldsymbol{\varphi}_\Gamma^{(L)}$ and $\boldsymbol{\varphi}_\Gamma^{(R)}$ we denote the values of $\boldsymbol{\varphi}$ on $\Gamma$ considered from the interior and the exterior of $K_\Gamma^{(L)}$, respectively, and set

$$\langle\boldsymbol{\varphi}\rangle_\Gamma = (\boldsymbol{\varphi}_\Gamma^{(L)} + \boldsymbol{\varphi}_\Gamma^{(R)})/2, \quad [\boldsymbol{\varphi}]_\Gamma = \boldsymbol{\varphi}_\Gamma^{(L)} - \boldsymbol{\varphi}_\Gamma^{(R)}. \tag{21}$$

The discrete problem is derived in the following way: We multiply system (3) by a test function $\boldsymbol{\varphi}_h \in \boldsymbol{S}_{ht}$, integrate over $K \in \mathcal{T}_{ht}$, apply Green's theorem, sum over all elements $K \in \mathcal{T}_{ht}$, use the concept of the numerical flux and introduce suitable terms mutually vanishing for a regular exact solution. Moreover, we carry out a linearization of nonlinear terms. In a similar way as in [6] we define the following forms.

*Convection form*: We set $\mathbb{A}_s(\boldsymbol{w}) = D\boldsymbol{f}_s(\boldsymbol{w})/D\boldsymbol{w}$, which is the Jacobi matrix of the mapping $\boldsymbol{f}_s$. Then $\frac{D\boldsymbol{g}_s(\boldsymbol{w})}{D\boldsymbol{w}} = \mathbb{A}_s(\boldsymbol{w}) - z_s\mathbb{I}$, and we write

$\mathbb{P}_g(\boldsymbol{w},\boldsymbol{n}) = \sum_{s=1}^{2} \frac{D\boldsymbol{g}_s(\boldsymbol{w})}{D\boldsymbol{w}} n_s = \sum_{s=1}^{2} (\mathbb{A}_s(\boldsymbol{w}) n_s - z_s n_s \mathbb{I})$. By [5], this matrix is diagonalizable. It means that there exists a nonsingular matrix $\mathbb{T} = \mathbb{T}(\boldsymbol{w},\boldsymbol{n})$ such that $\mathbb{P}_g = \mathbb{T}\Lambda\mathbb{T}^{-1}$, $\Lambda = \mathrm{diag}(\lambda_1,\dots,\lambda_4)$ where $\lambda_i = \lambda_i(\boldsymbol{w},\boldsymbol{n})$ are eigenvalues of the matrix $\mathbb{P}_g$. Further, we define the "positive" and "negative" parts of the matrix $\mathbb{P}_g$ by $\mathbb{P}_g^{\pm} = \mathbb{T}\Lambda^{\pm}\mathbb{T}^{-1}$, $\Lambda^{\pm} = \mathrm{diag}(\lambda_1^{\pm},\dots,\lambda_4^{\pm})$, where $\lambda^+ = \max(\lambda,0)$, $\lambda^- = \min(\lambda,0)$. Now, in the same way as in [6], for $\overline{\boldsymbol{w}}_h, \boldsymbol{w}_h, \boldsymbol{\varphi}_h \in \boldsymbol{S}_{ht}$ we define the linearized convection form

$$
\begin{aligned}
&\hat{b}_h(\overline{\boldsymbol{w}}_h, \boldsymbol{w}_h, \boldsymbol{\varphi}_h) \qquad (22)\\
&= -\sum_{K\in\mathcal{T}_{ht_{k+1}}} \int_K \sum_{s=1}^{2} (\mathbb{A}_s(\overline{\boldsymbol{w}}_h) - z_s(x))\mathbb{I})\boldsymbol{w}_h)\cdot \frac{\partial \boldsymbol{\varphi}_h}{\partial x_s}\,\mathrm{d}\boldsymbol{x}\\
&+ \sum_{\Gamma\in\mathcal{F}_{ht}^I} \int_\Gamma \Big(\mathbb{P}_g^+\big(\langle\overline{\boldsymbol{w}}_h\rangle, \boldsymbol{n}_\Gamma\big)\boldsymbol{w}_h^{(L)} + \mathbb{P}_g^-\big(\langle\overline{\boldsymbol{w}}_h\rangle, \boldsymbol{n}_\Gamma\big)\boldsymbol{w}_h^{(R)}\Big)\cdot[\boldsymbol{\varphi}_h]\,\mathrm{d}S\\
&+ \sum_{\Gamma\in\mathcal{F}_{ht}^B} \int_\Gamma \Big(\mathbb{P}_g^+\big(\langle\overline{\boldsymbol{w}}_h\rangle, \boldsymbol{n}_\Gamma\big)\boldsymbol{w}_h^{(L)} + \mathbb{P}_g^-\big(\langle\overline{\boldsymbol{w}}_h\rangle, \boldsymbol{n}_\Gamma\big)\overline{\boldsymbol{w}}_h^{(R)}\Big)\cdot\boldsymbol{\varphi}_h\,\mathrm{d}S.
\end{aligned}
$$

If $\Gamma\in\mathcal{F}_{ht}^B$, it is necessary to specify the boundary state $\overline{\boldsymbol{w}}_{h\Gamma}^{(R)}$ appearing in the numerical flux $\boldsymbol{H}_g$ in the definition of the inviscid form $\hat{b}_h$. Here we use the approach applied in the case of inviscid flow simulation, treated in [5], using a linearized initial-boundary value 1D Riemann problem.

*Viscous form*: The linearization of the viscous terms is based on the fact that $\boldsymbol{R}_s(\boldsymbol{w}_h, \nabla\boldsymbol{w}_h)$ is linear in $\nabla\boldsymbol{w}$ and nonlinear in $\boldsymbol{w}$. We get the linearized viscous form

$$
\begin{aligned}
\hat{a}_h(\overline{\boldsymbol{w}}_h, \boldsymbol{w}_h, \boldsymbol{\varphi}_h) &= \sum_{K\in\mathcal{T}_{ht}} \int_K \sum_{s=1}^{2} \boldsymbol{R}_s(\overline{\boldsymbol{w}}_h, \nabla\boldsymbol{w}_h)\cdot\frac{\partial\boldsymbol{\varphi}_h}{\partial x_s}\,\mathrm{d}\boldsymbol{x} \qquad (23)\\
&- \sum_{\Gamma\in\mathcal{F}_{ht}^I} \int_\Gamma \sum_{s=1}^{2} \big\langle \boldsymbol{R}_s(\overline{\boldsymbol{w}}_h, \nabla\boldsymbol{w}_h)\big\rangle(\boldsymbol{n}_\Gamma)_s\cdot[\boldsymbol{\varphi}_h]\,\mathrm{d}S\\
&- \sum_{\Gamma\in\mathcal{F}_{ht}^D} \int_\Gamma \sum_{s=1}^{2} \boldsymbol{R}_s(\overline{\boldsymbol{w}}_h, \nabla\boldsymbol{w}_h)(\boldsymbol{n}_\Gamma)_s\cdot\boldsymbol{\varphi}_h\,\mathrm{d}S.
\end{aligned}
$$

(We use the so-called incomplete version of the approximation of the viscous terms.)

*Interior and boundary penalty and righ-hand side forms*: Further, we set

$$J_h(\boldsymbol{w},\boldsymbol{\varphi}_h) = \sum_{\Gamma\in\mathcal{F}_{ht}^I}\int_\Gamma \sigma[\boldsymbol{w}]\cdot[\boldsymbol{\varphi}_h]\,dS + \sum_{\Gamma\in\mathcal{F}_{ht}^D}\int_\Gamma \sigma\boldsymbol{w}\cdot\boldsymbol{\varphi}_h\,dS, \tag{24}$$

$$\ell_h(\boldsymbol{w},\boldsymbol{\varphi}_h) = \sum_{\Gamma\in\mathcal{F}_{ht}^D}\int_\Gamma \sum_{s=1}^{2}\sigma\boldsymbol{w}_B\cdot\boldsymbol{\varphi}_h\,dS. \tag{25}$$

Here $\sigma|_\Gamma = C_W\mu/d(\Gamma)$ and $C_W > 0$ is a sufficiently large constant. The boundary state $\boldsymbol{w}_B$ is defined on the basis of the Dirichlet boundary conditions (7), a), b), d) and extrapolation:

$$\boldsymbol{w}_B = (\rho_D, \rho_D v_{D1}, \rho_D v_{D2}, c_v\rho_D\theta_\Gamma^{(L)} + \frac{1}{2}\rho_D|\boldsymbol{v}_D|^2) \quad \text{on } \Gamma_I, \tag{26}$$

$$\boldsymbol{w}_B = \boldsymbol{w}_\Gamma^{(L)} \quad \text{on } \Gamma_O, \tag{27}$$

$$\boldsymbol{w}_B = (\rho_\Gamma^{(L)}, \rho_\Gamma^{(L)} z_{D1}, \rho_\Gamma^{(L)} z_{D2}, c_v\rho_\Gamma^{(L)}\theta_\Gamma^{(L)} + \frac{1}{2}\rho_\Gamma^{(L)}|\boldsymbol{z}_D|^2) \quad \text{on } \Gamma_{W_t}. \tag{28}$$

*Reaction form* reads

$$d_h(\boldsymbol{w},\boldsymbol{\varphi}_h) = \sum_{K\in\mathcal{T}_{ht}}\int_K (\boldsymbol{w}\cdot\boldsymbol{\varphi}_h)\,\mathrm{div}\boldsymbol{z}\,\mathrm{d}\boldsymbol{x}. \tag{29}$$

*3.1.2. Time discretization*

Let us construct a partition $0 = t_0 < t_1 < t_2 \ldots$ of the time interval $[0,T]$ and define the time step $\tau_k = t_{k+1} - t_k$. We use the approximations $\boldsymbol{w}_h(t_n) \approx \boldsymbol{w}_h^n \in \boldsymbol{S}_{ht_n}$, $\boldsymbol{z}(t_n) \approx \boldsymbol{z}^n$, $n = 0, 1, \ldots$, and introduce the function $\hat{\boldsymbol{w}}_h^k = \boldsymbol{w}_h^k \circ \mathcal{A}_{t_k} \circ \mathcal{A}_{t_{k+1}}^{-1}$, which is defined in the domain $\Omega_{ht_{k+1}}$. The ALE derivative at time $t_{k+1}$ is approximated by the first- or second-order backward finite difference

$$\frac{D^A\boldsymbol{w}_h}{Dt}(x,t_{k+1}) \approx \frac{\boldsymbol{w}_h^{k+1}(x) - \hat{\boldsymbol{w}}_h^k(x)}{\tau_k}, \tag{30}$$

or

$$\frac{D^A\boldsymbol{w}_h}{Dt}(t_{k+1}) \approx \frac{2\tau_k+\tau_{k-1}}{\tau_k(\tau_k+\tau_{k-1})}\boldsymbol{w}_h^{k+1} - \frac{\tau_k+\tau_{k-1}}{\tau_k\tau_{k-1}}\hat{\boldsymbol{w}}_h^k + \frac{\tau_k}{\tau_{k-1}(\tau_k+\tau_{k-1})}\hat{\boldsymbol{w}}_h^{k-1}. \tag{31}$$

By the symbol $(\cdot,\cdot)$ we shall denote the scalar product in $L^2(\Omega_{ht_{k+1}})$, i.e.

$$(\boldsymbol{w}_h, \boldsymbol{\varphi}_h) = \int_{\Omega_{ht_{k+1}}} \boldsymbol{w}_h \cdot \boldsymbol{\varphi}_h \,\mathrm{d}\boldsymbol{x}, \tag{32}$$

respectively.

In order to avoid spurious oscillations in the approximate solution in the vicinity of discontinuities or steep gradients, we apply artificial viscosity forms introduced in [7]. They are based on the discontinuity indicator

$$g^k(K) = \int_{\partial K} [\hat\rho_h^k]^2 \,\mathrm{d}S \big/ (h_K |K|^{3/4}), \quad K \in \mathcal{T}_{ht_{k+1}}. \tag{33}$$

By $[\hat\rho_h^k]$ we denote the jump of the function $\hat\rho_h^k$ on the boundary $\partial K$ and $|K|$ denotes the area of the element $K$. Then for each $K \in \mathcal{T}_{ht_{k+1}}$ we define the discrete discontinuity indicator $G^k(K) = 0$ if $g^k(K) < 1$, $G^k(K) = 1$ if $g^k(K) \geq 1$ and the artificial viscosity forms

$$\hat\beta_h(\hat{\boldsymbol{w}}_h^k, \boldsymbol{w}_h^{k+1}, \boldsymbol{\varphi}_h) = \nu_1 \sum_{K\in\mathcal{T}_{ht_{k+1}}} h_K G^k(K) \int_K \nabla \boldsymbol{w}_h^{k+1} \cdot \nabla \boldsymbol{\varphi}_h \,\mathrm{d}\boldsymbol{x}, \tag{34}$$

$$\hat J_h(\hat{\boldsymbol{w}}_h^k, \boldsymbol{w}_h^{k+1}, \boldsymbol{\varphi}_h) = \nu_2 \sum_{\Gamma\in\mathcal{F}^I_{ht_{k+1}}} \frac{1}{2}\big(G^k(K_\Gamma^{(L)}) + G^k(K_\Gamma^{(R)})\big) \int_\Gamma [\boldsymbol{w}_h^{k+1}] \cdot [\boldsymbol{\varphi}_h] \,\mathrm{d}\mathcal{S},$$

with parameters $\nu_1$, $\nu_2 = O(1)$.

Finally, by $\overline{\boldsymbol{w}}_h^{k+1}$ we denote the state obtained by the extrapolation:

$$\overline{\boldsymbol{w}}_h^{k+1} = \hat{\boldsymbol{w}}_h^k \;\text{ and }\; \overline{\boldsymbol{w}}_h^{k+1} = \frac{\tau_k + \tau_{k-1}}{\tau_{k-1}} \hat{\boldsymbol{w}}_h^k - \frac{\tau_k}{\tau_{k-1}} \hat{\boldsymbol{w}}_h^{k-1} \tag{35}$$

in the case of the first-order time discretization and second-order time discretization, respectively.

The resulting scheme has the following form: For each $k = 0, 1, \ldots$ we seek $\boldsymbol{w}_h^{k+1} \in \boldsymbol{S}_{ht_{k+1}}$ such that

$$\begin{aligned}
&\Big(\frac{\boldsymbol{w}_h^{k+1} - \hat{\boldsymbol{w}}_h^k}{\tau_k}, \boldsymbol{\varphi}_h\Big) + \hat b_h(\overline{\boldsymbol{w}}_h^{k+1}, \boldsymbol{w}_h^{k+1}, \boldsymbol{\varphi}_h) + \hat a_h(\overline{\boldsymbol{w}}_h^{k+1}, \boldsymbol{w}_h^{k+1}, \boldsymbol{\varphi}_h) \\
&+ J_h(\boldsymbol{w}_h^{k+1}, \boldsymbol{\varphi}_h) + d_h(\boldsymbol{w}_h^{k+1}, \boldsymbol{\varphi}_h) + \hat\beta_h(\hat{\boldsymbol{w}}_h^k, \boldsymbol{w}_h^{k+1}, \boldsymbol{\varphi}_h) \\
&+ \hat J_h(\hat{\boldsymbol{w}}_h^k, \boldsymbol{w}_h^{k+1}, \boldsymbol{\varphi}_h) = \ell(\overline{\boldsymbol{w}}_B^{k+1}, \boldsymbol{\varphi}_h), \quad \forall \boldsymbol{\varphi}_h \in \boldsymbol{S}_{ht_{k+1}},
\end{aligned} \tag{36}$$

in the case of the first-order time discretization. In the case of the second-order time discretization the expression $(\boldsymbol{w}_h^{k+1} - \hat{\boldsymbol{w}}_h^k, \boldsymbol{\varphi}_h)/\tau_k$ is replaced by by the approximation (31).

*3.2. Discretization of the structural problem*

*3.2.1. Space semidiscretization*

The space semidiscretization of the structural problem will be carried out by the conforming finite element method. By $\Omega_h^b$ we denote a polygonal approximation of the domain $\Omega^b$. We construct a triangulation $\mathcal{T}_h^b$ of the domain $\Omega_h^b$ formed by a finite number of closed triangles with the following properties:

a) $\overline{\Omega}_h^b = \bigcup_{K\in\mathcal{T}_h^b} K$.

b) The intersection of two different elements $K, K' \in \mathcal{T}_h^b$ is either empty or a common edge of these elements or their common vertex.

c) The vertices lying on $\partial\Omega_h^b$ are elements of $\partial\Omega^b$.

d) The set $\overline{\Gamma}_W^b \cap \overline{\Gamma}_D^b$ is formed by vertices of some elements $K \in \mathcal{T}_h^b$.

Further, by $\Gamma_{Wh}^b$ and $\Gamma_{Dh}^b$ we denote the parts of $\partial\Omega_h^b$ approximating $\Gamma_W^b$ and $\Gamma_D^b$.

The approximate solution of the structural problem will be sought in the finite-dimensional space $\boldsymbol{X_h} = X_h \times X_h$, where

$$X_h = \left\{ v_h \in C(\overline{\Omega}_h^b);\ v_h|_K \in P_s(K),\ \forall K \in \mathcal{T}_h^b \right\} \tag{37}$$

and $s \geq 1$ is an integer. In $\boldsymbol{X}_h$ we define the subspace $\boldsymbol{V_h} = V_h \times V_h$, where

$$V_h = \left\{ y_h \in X_h; y_h|_{\overline{\Gamma}_{Dh}^b} = 0 \right\}. \tag{38}$$

The derivation of the space semidiscretization can be obtained in a standard way. Multiplying system (8) by any test function $y_{hi} \in V_h,\ i = 1, 2$, applying Green's theorem and using the boundary condition (13), we obtain an identity containing the forms defined for $\boldsymbol{u}_h = (u_{h1}, u_{h2}),\ \boldsymbol{y}_h = (y_{h1}, y_{h2}) \in \boldsymbol{X}_h$:

$$a_h(\boldsymbol{u}_h, \boldsymbol{y}_h) = \int_{\Omega_h^b} \lambda^b \mathrm{div}\, \boldsymbol{u}_h \,\mathrm{div}\, \boldsymbol{y}_h \,\mathrm{d}\boldsymbol{X} + 2\int_{\Omega_h^b} \mu^b \sum_{i,j=1}^{2} e_{ij}^b(\boldsymbol{u}_h)\, e_{ij}^b(\boldsymbol{y}_h)\,\mathrm{d}\boldsymbol{X}, \tag{39}$$

and

$$(\boldsymbol{\varphi}, \boldsymbol{\psi})_{\Omega_h^b} = \int_{\Omega_h^b} \boldsymbol{\varphi}\cdot\boldsymbol{\psi}\,\mathrm{d}\boldsymbol{X}, \quad (\boldsymbol{\varphi}, \boldsymbol{\psi})_{\Gamma_{Wh}} = \int_{\Gamma_{Wh}} \boldsymbol{\varphi}\cdot\boldsymbol{\psi}\,\mathrm{d}S. \tag{40}$$

We shall use the approximation $\boldsymbol{T}_h^{\boldsymbol{n}} \approx \boldsymbol{T}^{\boldsymbol{n}}$ and the notation $\boldsymbol{u}_h'(t) = \frac{\partial \boldsymbol{u}_h(t)}{\partial t}$ and $\boldsymbol{u}_h''(t) = \frac{\partial^2 \boldsymbol{u}_h(t)}{\partial t^2}$. Then we define the *approximate solution of the structural*

*problem* as a function $t \in [0,T] \to \boldsymbol{u}_h(t) \in \boldsymbol{V}_h$ such that there exist the derivatives $\boldsymbol{u}_h'(t)$, $\boldsymbol{u}_h''(t)$ and the identity

$$(\varrho^b \boldsymbol{u}_h''(t), \boldsymbol{y}_h)_{\Omega_h^b} + (C\varrho^b \boldsymbol{u}_h'(t), \boldsymbol{y}_h)_{\Omega_h^b} + a_h(\boldsymbol{u}_h(t), \boldsymbol{y}_h) = (\boldsymbol{T}_h^{\boldsymbol{n}}(t), \boldsymbol{y}_h)_{\Gamma_{Wh}}, \\ \forall \boldsymbol{y}_h \in \boldsymbol{V}_h, \quad \forall t \in (0,T), \quad (41)$$

and the initial conditions

$$\boldsymbol{u}_h(\boldsymbol{X},0) = 0, \quad \boldsymbol{u}_h'(\boldsymbol{X},0) = 0, \quad \boldsymbol{X} \in \Omega_h^b. \quad (42)$$

are satisfied.

The discrete problem (41), (42) is equivalent to the solution of a system of ordinary differential equations. Let functions $\varphi_1, \ldots, \varphi_m$ form a basis of the space $V_h$. Then the system of $n = 2m$ of the vector functions $(\varphi_1, 0), \ldots, (\varphi_m, 0), (0, \varphi_1), \ldots, (0, \varphi_m)$ form a basis of the space $\boldsymbol{V}_h$. Let us denote them by $\boldsymbol{\varphi}_1, \ldots \boldsymbol{\varphi}_n$. Then the approximate solution $\boldsymbol{u}_h$ can be expressed in the form

$$\boldsymbol{u}_h(t) = \sum_{j=1}^{n} p_j(t) \boldsymbol{\varphi}_j, \quad t \in [0,T]. \quad (43)$$

Let us set $\boldsymbol{p}(t) = (p_1(t), \ldots, p_n(t))$. Using $\boldsymbol{\varphi}_j$, $j = 1, \ldots, n$, as test functions in (41), we get the following system of ordinary differential equations

$$\mathbb{M}\boldsymbol{p}'' = \boldsymbol{G} - \mathbb{K}\boldsymbol{p} - C\mathbb{M}\boldsymbol{p}', \quad (44)$$

where $\mathbb{M} = (m_{ij})_{i,j=1}^n$ is the mass matrix and $\mathbb{K} = (k_{ij})_{i,j=1}^n$ is the stiffness matrix with the elements $m_{ij} = (\rho^b \boldsymbol{\varphi}_i, \boldsymbol{\varphi}_j)$ and $k_{ij} = a_h(\boldsymbol{\varphi}_i, \boldsymbol{\varphi}_j)$, respectively. The aerodynamic force vector $\boldsymbol{G} = \boldsymbol{G}(t) = (G_1(t), \ldots, G_n(t))^T$ has the components $G_i(t) = (\boldsymbol{T}_h^n(t), \boldsymbol{\varphi}_i)_{\Gamma_{Wh}}$, $i = 1, \ldots, n$. System (44) is equipped with the initial conditions

$$p_j(0) = 0, \quad p_j'(0) = 0, \quad j = 1, \ldots, n. \quad (45)$$

*3.2.2. Time discretization of the structural problem*

The discrete initial value problem (44), (45) is solved by the Newmark method ([4]). We consider the partition of the time interval $[0,T]$ formed by the time instants $0 = t_0 < t_1 < \ldots$ introduced in Section 3.1.2. Let us set $\boldsymbol{p}_0 = 0, \boldsymbol{z}_0 = 0, \boldsymbol{G}_k = \boldsymbol{G}(t_k)$, and introduce the approximations $\boldsymbol{p}_k \approx \boldsymbol{p}(t_k)$

and $\boldsymbol{q}_k \approx \boldsymbol{p}'(t_k)$ for $k = 1, 2, \ldots$ . The Newmark scheme can be written in the form

$$\begin{aligned} \boldsymbol{p}_{k+1} &= \boldsymbol{p}_k + \tau_k \boldsymbol{q}_k + \tau_k^2 \Big( \beta \left( \mathbb{M}^{-1} \boldsymbol{G}_{k+1} - \mathbb{M}^{-1} \mathbb{K} \boldsymbol{p}_{k+1} - C \boldsymbol{q}_{k+1} \right) \\ &\quad + \left( \frac{1}{2} - \beta \right) \left( \mathbb{M}^{-1} \boldsymbol{G}_k - \mathbb{M}^{-1} \mathbb{K} \boldsymbol{p}_k - C \boldsymbol{q}_k \right) \Big), \end{aligned} \tag{46}$$

$$\begin{aligned} \boldsymbol{q}_{k+1} &= \boldsymbol{q}_k + \tau_k \Big( \gamma \left( \mathbb{M}^{-1} \boldsymbol{G}_{k+1} - \mathbb{M}^{-1} \mathbb{K} \boldsymbol{p}_{k+1} - C \boldsymbol{q}_{k+1} \right) \\ &\quad + (1 - \gamma) \left( \mathbb{M}^{-1} \boldsymbol{G}_k - \mathbb{M}^{-1} \mathbb{K} \boldsymbol{p}_k - C \boldsymbol{q}_k \right) \Big), \end{aligned} \tag{47}$$

where $\beta, \gamma \in \mathbb{R}$ are parameters. From equation (47) we get

$$\begin{aligned} \boldsymbol{q}_{k+1} &= \frac{1}{1 + C\gamma\tau_k} \Big( \boldsymbol{q}_k + \tau_k \Big( \gamma \left( \mathbb{M}^{-1} \boldsymbol{G}_{k+1} - \mathbb{M}^{-1} \mathbb{K} \boldsymbol{p}_{k+1} \right) \\ &\quad + (1 - \gamma) \left( \mathbb{M}^{-1} \boldsymbol{G}_k - \mathbb{M}^{-1} \mathbb{K} \boldsymbol{p}_k - C \boldsymbol{q}_k \right) \Big) \Big). \end{aligned} \tag{48}$$

The substitution of (48) in (46) yields the relation which can be written in the form

$$\begin{aligned} &\left( \mathbb{I} + \xi_k \mathbb{M}^{-1} \mathbb{K} \right) \boldsymbol{p}_{k+1} = \boldsymbol{p}_k + (\tau_k - C\xi_k) \, \boldsymbol{q}_k + \xi_k \mathbb{M}^{-1} \boldsymbol{G}_{k+1} + \\ &\quad + \left( C \left( \gamma - 1 \right) \xi_k \tau_k + \left( \frac{1}{2} - \beta \right) \tau_k^2 \right) \left( \mathbb{M}^{-1} \boldsymbol{G}_k - \mathbb{M}^{-1} \mathbb{K} \boldsymbol{p}_k - C \boldsymbol{q}_k \right). \end{aligned} \tag{49}$$

where we set for the sake of simplicity

$$\xi_k = \beta \tau_k^2 \left( 1 - \frac{C\gamma\tau_k}{1 + C\gamma\tau_k} \right) = \frac{\beta \tau_k^2}{1 + C\gamma\tau_k}. \tag{50}$$

If $\boldsymbol{p}_k$ and $\boldsymbol{q}_k$ are known, then $\boldsymbol{p}_{k+1}$ is obtained from system (49) and afterwards $\boldsymbol{q}_{k+1}$ is computed from (48).

In numerical examples presented in Section 5, the parameters $\beta = 1/4$ and $\gamma = 1/2$ were used. This choice yields the Newmark method of the second order.

## 4. Realization of the coupled FSI problem

In this section we shall describe the algorithm of the numerical realization of the complete fluid-structure interaction problem.

*4.1. Construction of the ALE mapping for fluid*

The ALE mapping is constructed with the aid of an artificial stationary elasticity problem. We seek $\boldsymbol{d} = (d_1, d_2)$ defined in $\Omega_0$ as a solution of the elastostatic system

$$\sum_{j=1}^{2} \frac{\partial \tau_{ij}^a}{\partial x_j} = 0 \quad \text{in } \Omega_0, \quad i = 1, 2, \tag{51}$$

where $\tau_{ij}^a$ are the components of the artificial stress tensor

$$\tau_{ij}^a = \lambda^a \mathrm{div}\, \boldsymbol{d}\, \delta_{ij} + 2\mu^a e_{ij}^a, \quad e_{ij}^a(\boldsymbol{d}) = \frac{1}{2}\left(\frac{\partial d_i}{\partial x_j} + \frac{\partial d_j}{\partial x_i}\right), \quad i, j = 1, 2. \tag{52}$$

The Lamé coefficients $\lambda^a$ and $\mu^a$ are related to the artificial Young modulus $E^a$ and to the artificial Poisson number $\sigma_a$ as in (11). The boundary conditions for $\boldsymbol{d}$ are prescribed by

$$\boldsymbol{d}|_{\Gamma_I \cup \Gamma_O} = 0, \ \boldsymbol{d}|_{\Gamma_{W0h} \setminus \Gamma_{Wh}} = 0, \ \boldsymbol{d}(\boldsymbol{x}, t) = \boldsymbol{u}(\boldsymbol{x}, t), \ \boldsymbol{x} \in \Gamma_{Wh}. \tag{53}$$

The solution of (51) gives us the ALE mapping of $\overline{\Omega}_0$ onto $\overline{\Omega}_t$ in the form

$$\mathcal{A}_t(\boldsymbol{x}) = \boldsymbol{x} + \boldsymbol{d}(\boldsymbol{x}, t), \quad \boldsymbol{x} \in \overline{\Omega}_0, \tag{54}$$

for each time $t$.

System (51) is discretized by the conforming piecewise linear finite elements on the mesh $\mathcal{T}_{h0}$ used for computing the flow field in the beginning of the computational process in the polygonal approximation $\Omega_{h0}$ of the domain $\Omega_0$. The use of linear finite elements is sufficient, because we need only to know the movement of the points of the mesh.

In our computations we choose the Lamé coefficients $\lambda^a$ and $\mu^a$ as constants corresponding to the Young modulus and Poisson ratio $E^a = 10000$ and $\sigma^a = 0.45$.

If the displacement $\boldsymbol{d}_h$ is computed at time $t_{k+1}$, then in view of (54), the approximation of the ALE mapping is obtained in the form

$$\mathcal{A}_{t_{k+1}h}(\boldsymbol{x}) = \boldsymbol{x} + \boldsymbol{d}_h(\boldsymbol{x}), \quad \boldsymbol{x} \in \Omega_{0h}. \tag{55}$$

The knowledge of the ALE mapping at the time instants $t_{k-1}$, $t_k$, $t_{k+1}$ allows us to approximate the domain velocity with the aid of the second-order backward difference formula

$$\boldsymbol{z}_h^{k+1}(\boldsymbol{x}) = \frac{3\boldsymbol{x} - 4\mathcal{A}_{t_k h}(\mathcal{A}_{t_{k+1}h}^{-1}(\boldsymbol{x})) + \mathcal{A}_{t_{k-1}h}(\mathcal{A}_{t_{k+1}h}^{-1}(\boldsymbol{x}))}{2\tau}, \quad \boldsymbol{x} \in \Omega_{t_{k+1}h}. \tag{56}$$

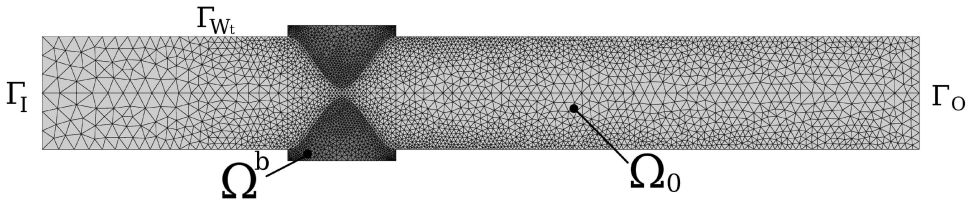


Figure 1: Computational domain at time $t = 0$ with a finite element mesh.

*4.2. Coupling procedure*

In the solution of the complete coupled fluid-structure interaction problem it is necessary to apply a suitable coupling procedure. See, e.g. [3] for a general framework. Here we apply the following algorithm.

1. Assume that the approximate solution of the flow problem on the time level $t_k$ is known as well as the deformation of the structure $\boldsymbol{u}_{h,k}$.
2. Set $\boldsymbol{u}^0_{h,k+1} := \boldsymbol{u}_{h,k},\ l := 1$ and apply the iterative process:
   (a) Compute the stress tensor $\tau^f_{ij}$ and the aerodynamical force acting on the structure and transform it to the interface $\Gamma^b_{Wh}$.
   (b) Solve the elasticity problem, compute the deformation $\boldsymbol{u}^l_{h,k+1}$ at time $t_{k+1}$ and approximate the domain $\Omega^l_{ht_{k+1}}$.
   (c) Determine the ALE mapping $\mathcal{A}^l_{t_{k+1}h}$ and approximate the domain velocity $\boldsymbol{z}^l_{h,k+1}$.
   (d) Solve the flow problem on the approximation of $\Omega^l_{ht_{k+1}}$.
   (e) If the variation of the displacement $\boldsymbol{u}^l_{h,k+1}$ and $\boldsymbol{u}^{l-1}_{h,k+1}$ is larger than the prescribed tolerance, go to a) and $l := l + 1$. Else $k := k + 1$ and goto 2).

This represents the so-called strong coupling. If in the step e) we set $k := k + 1$ and go to 2) already in the case when $l = 1$, then we get the weak (loose) coupling.

## 5. Numerical examples

In order to demonstrate the applicability of the developed method, we present here results of some numerical experiments.

We consider a model of flow through a channel with two bumps which represent time dependent boundaries between the flow and a simplified model

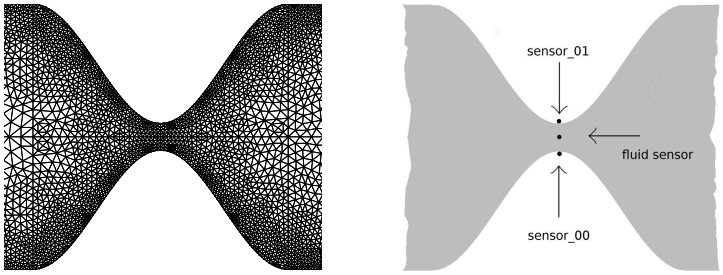


Figure 2: Detail of the flow computational mesh at time $t = 0$ near the narrowest part of the channel and the position of some sensors used in analysis.

of vocal folds (see Figures 1 and 2). The numerical experiments were carried out for the following data: magnitude of the inlet velocity $v_{in} = 4$ m/s, the fluid viscosity $\mu = 15 \cdot 10^{-6}\ \mathrm{kg\,m^{-1}\,s^{-1}}$, the inlet density $\rho_{in} = 1.225\ \mathrm{kg\,m^{-3}}$, the outlet pressure $p_{out} = 97611$ Pa, the Reynolds number $Re = \rho_{in} v_{in} H/\mu = 5227$, heat conduction coefficient $k = 2.428 \cdot 10^{-2}\,\mathrm{kg\,m\,s^{-2}\,K^{-1}}$, the specific heat $c_v = 721.428\,\mathrm{m^2\,s^{-2}\,K^{-1}}$, the Poisson adiabatic constant $\gamma = 1.4$. The inlet Mach number is $M_{in} = 0.012$. The Young modulus and the Poisson ratio have values $E^b = 25000$ Pa and $\sigma^b = 0.4$, respectively, the structural damping coefficient is equal to the constant $C = 100\ \mathrm{s^{-1}}$ and the material density $\rho^b = 1040\,\mathrm{kg\,m^{-3}}$ . The quadratic ($r = 2$) and linear ($s = 1$) elements were used for the approximation of flow and structural problem, respectively.

Figure 1 shows the situation at the initial time $t = 0$ the flow computational mesh consisting of 5398 elements and the strucure computational mesh with 1998 elements. In Figure 2 we see a detail of the flow mesh near the narrowest part of the channel at the initial time and the positions of sensor points used in the analysis.

First we tested the influence of the density of the computational meshes on the oscillations of the pressure averaged over the outlet $\Gamma_O$ and the corresponding Fourier analysis. We consider three successively refined meshes. Figure 3 shows the behaviour of the quantity

$$p_{av}(t) = \int_{\Gamma_O} \left( p(x,t) - \frac{1}{T} \int_0^T p(x,t)\,\mathrm{d}t \right) / \int_{\Gamma_O} \mathrm{d}S. \tag{57}$$

in dependence on time, computed on the flow/structure meshes with 5398/1998 elements (red), 10130/2806 elements (green) and 20484/4076 elements (blue)

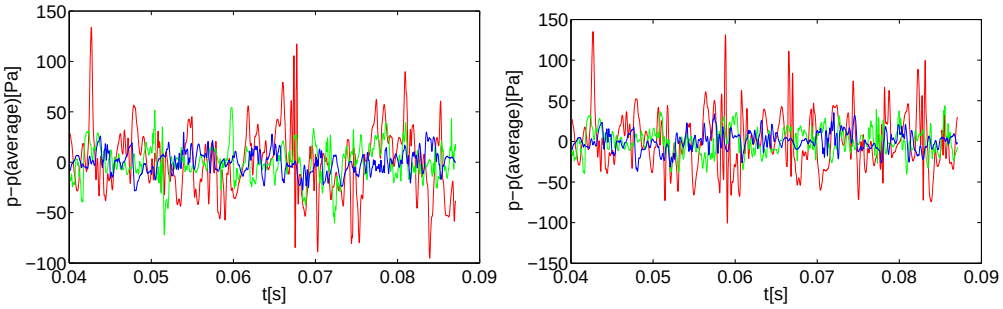


Figure 3: Dependence of the quantity $p_{av}$ computed on three meshes: strong coupling (left), weak coupling (right).

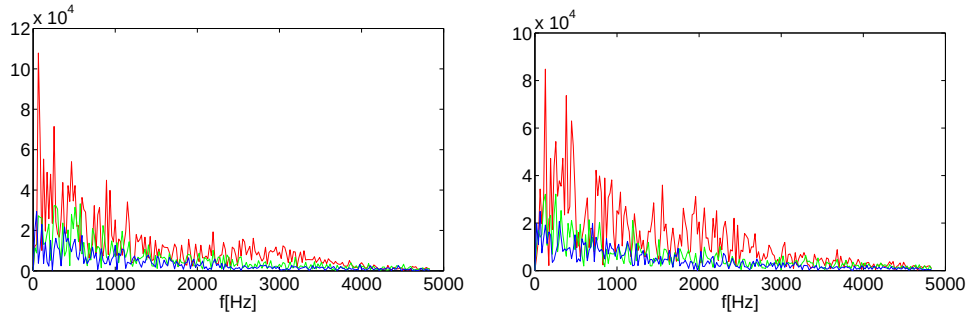


Figure 4: Fourier analysis of the quantity $p_{av}$ computed on three meshes: strong coupling (left), weak coupling (right).

with the aid of the strong coupling (left) and the weak coupling (right). Figure 4 shows the corresponding Fourier analysis. During the successive mesh refinement one can observe the convergence tendency manifested by the decrease of the magnitude of the quantity $p_{av}$ fluctuations and the decrease of the magnitude of the Fourier spectra. No peaks related to any basic acoustic modes of vibration in the channel were identified in the spectra. The difference between the results obtained by the strong and weak coupling is not too large. The main difference is in a higher stability of the strong coupling during solving the problem on a long time interval. On the other hand, the strong coupling requires naturally longer CPU time.

Flow-induced deformations of the vocal folds model with the computational mesh and the velocity field near the vocal folds are shown in Figure 5 at several time instants. We can see the Coanda effect represented by the attachment of the main stream (jet) successively to the upper and lower wall

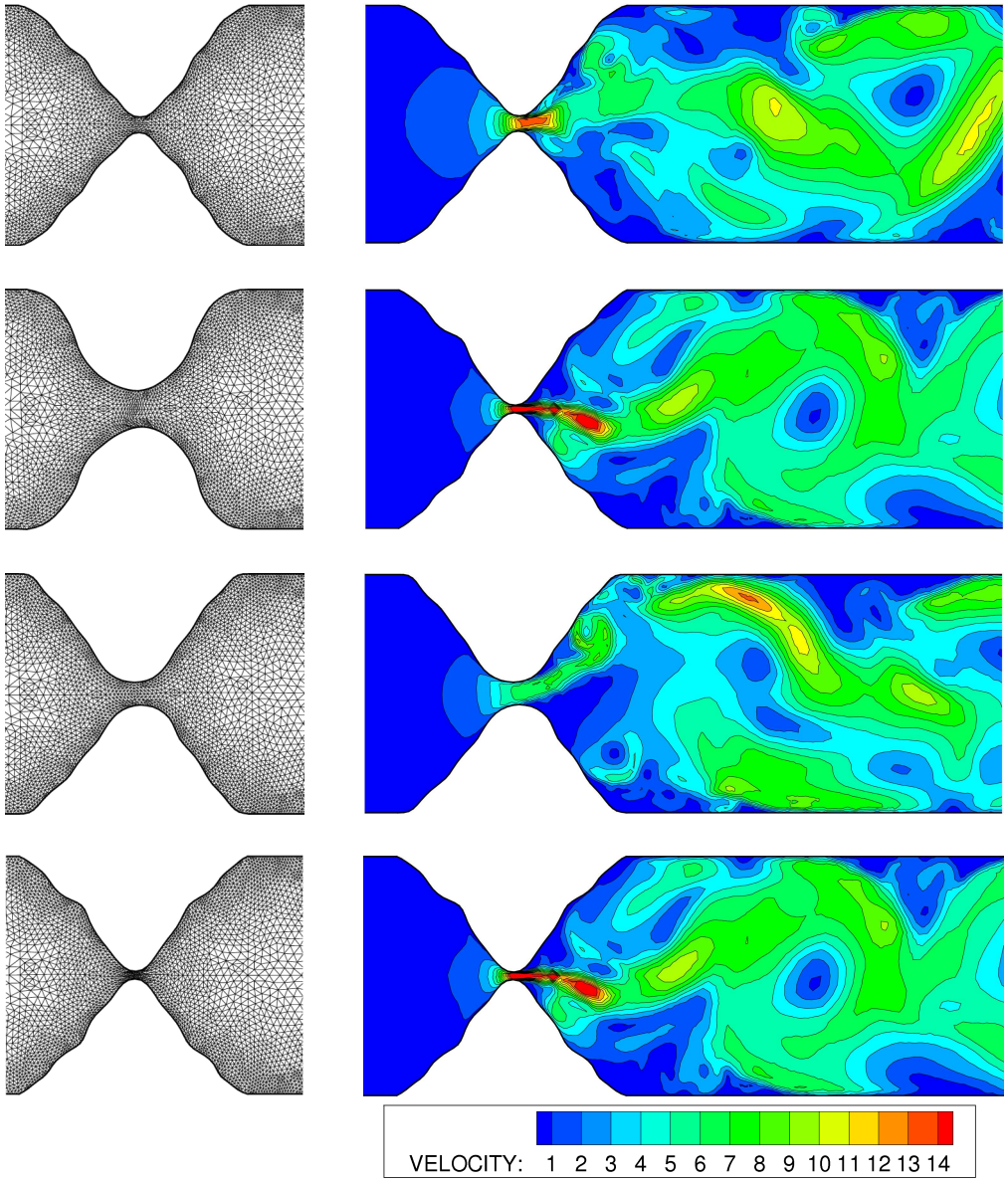


Figure 5: Detail of the mesh and the velocity distribution in the vicinity of the narrowest part of the channel at time instants $t = 0.2656, 0.2672, 0.2688, 0.2704$ s.

and formation of large scale vortices behind the glottis. The character of the vocal folds vibration can be indicated in Figure 6, which shows the displacements of the sensor points on the vocal folds surface (marked in Figure 2) and the fluid pressure fluctuations in the middle of the gap as well as the Fourier analysis of the signals. The vocal folds vibrations are not symmetric due to the Coanda effect and are composed of the fundamental horizontal mode of vibration with the corresponding eigen-frequency 113 Hz and by the higher eigenmode with the eigenfrequency 439 Hz. The increase of horizontal vibrations due to the aeroelastic instability of the system results in a fast decrease of the glottal gap. At about $t = 0.2$ s, when the gap is nearly closed, the fluid mesh deformation in this region is too high and the numerical simulation stopped. The dominant peak at 439 Hz in the spectrum of the pressure signal corresponds well to the vertical oscillations of the glottal gap, while the importance of the lower frequency 113 Hz associated with the horizontal vocal folds motion is in the pressure fluctuations negligible. The modeled flow-induced instability of the vocal folds is called phonation onset followed in reality by a complete closing of the glottis and consequently by the vocal folds collisions producing the voice source acoustic signal.

## 6. Conclusion

We have presented a robust higher-order method for the numerical simulation of the interaction of compressible flow with elastic structures with applications to the computation of flow-induced vibrations of vocal folds during phonation. It is based on several important ingredients:

- the ALE method applied to the compressible Navier-Stokes equations,
- the application of the discontinuous Galerkin method for the space discretization and semi-implicit linearized time discretization,
- the use of conforming finite elements for the space discretization and of the Newmark method for the time discretization of the elasticity problem,
- technique for the construction of the ALE mapping,
- the application of coupling algorithms for the realization of the coupled FSI problem.

The numerical tests and experiments show that the developed method can be applied to the numerical solution of the interaction of compressible flow

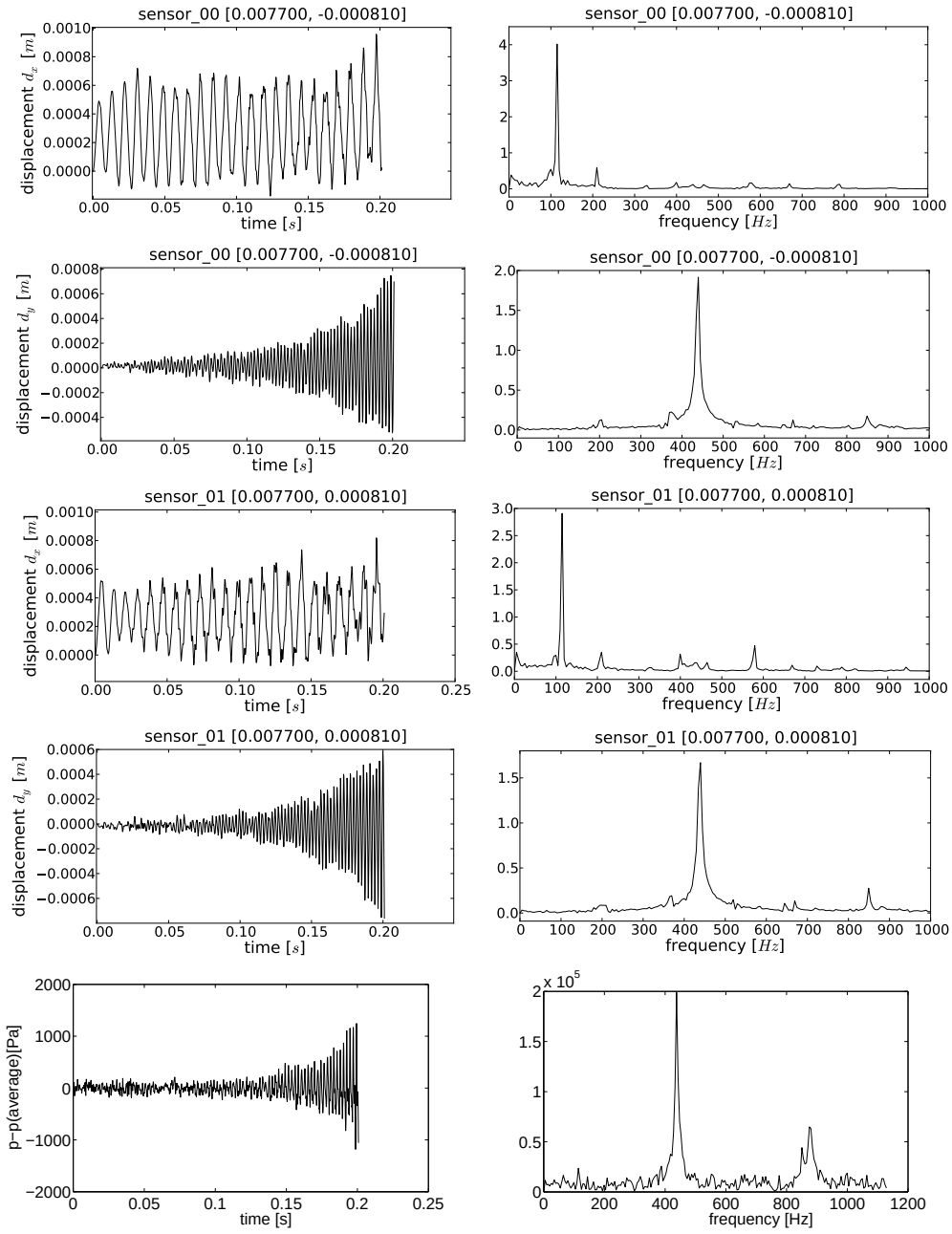


Figure 6: Vibrations of sensor points lying on the boundary of the vocal folds and the pressure oscillations in the middle of the gap (left), and the corresponding Fourier analyses (right).

and elastic structures with applications to the simulation of air flow through vocal folds.

Future work will be concentrated on the following topics:

- further analysis of the robustness and accuracy of the method with respect to the Mach number and Reynolds number,
- investigation of various types of boundary conditions,
- the realization of a remeshing in the case of closing the glottal channel during the oscillation period of the channel walls,
- the use of nonlinear elasticity models including vocal folds collision,
- the use of a suitable turbulence model,
- the identification of the acoustic signal.

**Acknowledgements** This work was supported by the grants No. 201/08/0012 (M. Feistauer, V. Kučera) and P101/11/0207 (J. Horáček) of the Czech Science Foundation, and by the grants SVV-2010-261316 and GAChU 549912 financed by the Charles University in Prague (J. Hasnedlová-Prokopová and A. Kosík).

## References

[1] F. Alipour, I. R. Titze, Combined simulation of two-dimensional airflow and vocal fold vibration. In: P. J. Davis and N. H. Fletcher, editors. Vocal fold physiology, controlling complexity and chaos, San Diego (1996).

[2] F. Alipour, Ch. Brücker, D.D. Cook, A. Gömmel, M. Kaltenbacher, W. Mattheus, L. Mongeau, E. Nauman, R. Schwarze, I. Tokuda and S. Zörner, Mathematical models and numerical schemes for the simulation of human phonation, Current Bioinformatics, 6, 323-343 (2011).

[3] S. Badia, R. Codina, On some fluid-structure iterative algorithms using pressure segregation methods. Application to aeroelasticity, *Int. J. Numer. Meth. Engng*, **72**, 46–71 (2007).

[4] A. Curnier, Computational Methods in Solid Mechanics, Kluwer Academic Publishing Group, Dodrecht (1994).

[5] M. Feistauer, J. Felcman and I. Straškraba, Mathematical and Computational Methods for Compressible Flow, *Clarendon Press*, Oxford (2003).

[6] M. Feistauer, J. Horáček, V. Kučera, J. Prokopová, On numerical solution of compressible flow in time-dependent domains, *Mathematica Bohemica*, 137 (2011), 1–16.

[7] M. Feistauer and V. Kučera, On a robust discontinuous Galerkin technique for the solution of compressible flow, *J. Comput. Phys.*, **224**, 208–221 (2007).

[8] J. Horáček and J. G. Švec, Aeroelastic model of vocal-fold-shaped vibrating element for studying the phonation threshold, *J. Fluids Struct.*, **16**, 931-955 (2002).

[9] J. Horáček, P. Šidlof and J. G. Švec, Numerical simulation of self-oscillations of human vocal folds with Hertz model of impact forces, *J. Fluids Struct.*, **20**, 853-69 (2005).

[10] T. Nomura and T.J.R. Hughes, An arbitrary Lagrangian-Eulerian finite element method for interaction of fluid and a rigid body, *Comput. Methods Appl. Mech. Engrg.*, **95**, 115-138 (1992).

[11] P. Punčochářová-Pořízková, K. Kozel and J. Horáček, Simulation of unsteady compressible flow in a channel with vibrating walls - influence of the frequency, *Computers and Fluids*, **46**, 404-410 (2011).

[12] P. Sváček, M. Feistauer and J. Horáček, Numerical simulation of flow induced airfoil vibrations with large amplitudes. *J. Fluids Struct.*, **23**, 391-411 (2007).

[13] I.R. Titze, Principles of Voice Production, National Centre for Voice and Speech, Iowa City (2000).

[14] I.R. Titze, The Myoelastic Aerodynamic Theory of Phonation, National Centre for Voice and Speech, Denver and Iowa City (2006).

[15] M. P. De Vries, H. K. Schutte, A. E. P. Veldman and G. J. Verkerke, Glottal flow through a two-mass model: comparison of Navier-Stokes solutions with simplified models, *J. Acoust. Soc. Am.*, **111** (4), 1847-53 (2002).

[16] Z. Zhang, J. Neubauer and D. A. Berry, Physical mechanisms of phonation onset: A linear stability analysis of an aeroelastic continuum model of phonation, *J. Acoust. Soc. Am.*, **122**, 2279-2295 (2007).